ELSEVIER

Applied Catalysis A: General 171 (1998) 131–143

APPLIED CATALYSIS A: GENERAL

Cooperation effects towards partial oxidation of isobutene in multiphasic catalysts based on bismuth pyrostannate

L. Moens[a], P. Ruiz[b], B. Delmon[b], M. Devillers[a,*]

[a]*Laboratoire de Chimie Inorganique et Analytique, Université Catholique de Louvain, place Louis Pasteur, 1, B-1348 Louvain-la-Neuve, Belgium*

[b]*Unité de Catalyse et de Chimie des Matériaux Divisés, Université Catholique de Louvain, place Croix du Sud, 2, B-1348 Louvain-la-Neuve, Belgium*

Received 27 October 1997; received in revised form 19 February 1998; accepted 23 February 1998

Abstract

The catalytic behaviour of α-$Bi_2Sn_2O_7$ was investigated within the framework of the remote control theory. Mixtures of bismuth pyrostannate with typical oxygen donors (Bi_2O_3, Sb_2O_4) or acceptors (MoO_3, WO_3) were therefore prepared and tested in the isobutene–methacrolein conversion at 648 and 673 K. The catalysts were characterized before and after their use by X-ray diffractometry, X-ray photoelectron spectroscopy, scanning electron microscopy and BET specific surface area measurements. The experiments indicate that cooperation for partial oxidation occurs when $Bi_2Sn_2O_7$ is mixed with acceptor phases. Several mechanisms allowing to explain the synergetic effects observed in the $Bi_2Sn_2O_7$–WO_3 and the $Bi_2Sn_2O_7$–MoO_3 mixtures are discussed. In the $Bi_2Sn_2O_7$–WO_3 catalysts, arguments are presented showing that surface enrichment by one oxide or the in situ formation of a bismuth tungstate phase cannot be reasonably considered as responsible for the cooperation effects. Bismuth stannate is consequently concluded to behave as an oxygen donor with respect to WO_3. $Bi_2Sn_2O_7$ could ''a priori'' display the same behaviour in the $Bi_2Sn_2O_7$–MoO_3 catalysts and cooperate with MoO_3 via a remote control mechanism. But in the latter case, as α-$Bi_2Mo_3O_{12}$ is generated in situ, the intrinsic catalytic activity of this bismuth molybdate must probably be taken into account as an additional explanation for the synergy observed in these mixtures. On the other hand, the hypothesis of coverage of one oxide by the other one seems to be ruled out in these $Bi_2Sn_2O_7$–MoO_3 catalysts.

Keywords: Oxidation; Bismuth; Pyrostannate; Remote control

1. Introduction

Cooperative effects between separate oxide phases have been reported on many occasions in the field of partial oxidation of hydrocarbons [1,2]. They usually result, either in increased selectivities to given products, or in inhibition of deactivation, and have been rationalized mainly through four different mechanisms: (i) formation of a new (mixed) phase from the two initial phases in contact (this being possibly limited to the contact zone), (ii) epitaxial matching between selected crystal planes of the two oxides, (iii) surface contamination of one phase by metallic

*Corresponding author. Tel.: 0032 10-472 827; fax: 0032 10-472 836; e-mail: devillers@inan.ucl.ac.be

0926-860X/98/$19.00
PII S0926-860X(98)00075-1

elements from the other phase and (iv) a remote control mechanism based on the activation of molecular oxygen by a donor phase into mobile species (spill-over oxygen), which migrate to an acceptor phase, where they create and/or regenerate selective catalytic sites [2]. In the latter case, cooperation is achieved between two separate and non-contaminated phases.

Bismuth pyrostannate, α-$Bi_2Sn_2O_7$, has been mentioned as a catalyst in several partial oxidation reactions such as dehydrodimerization [3–5] or aromatic dehydroaromatization [6] of propene, selective oxidation of propene into acrolein [7], oxidative dehydrogenation of 1-butene into butadiene [6] and oxidative coupling of methane [8]. In a previous paper, we have shown that mixtures containing both $Bi_2Sn_2O_7$ and SnO_2 display high catalytic activity in the total oxidation of isobutene [9]. The present work is devoted to the study of the catalytic behaviour of the α-$Bi_2Sn_2O_7$ phase in the selective oxidation of isobutene to methacrolein and the catalytic potentialities of this ternary phase were investigated in the context of the remote control theory [10]. Mixtures of bismuth pyrostannate with typical oxygen donors like bismuth oxide, α-Bi_2O_3 [10] or antimony oxide, α-Sb_2O_4 [11], and with typical oxygen acceptors like molybdenum(VI) oxide, MoO_3 [11], or tungsten(VI) oxide, WO_3 [12], were therefore prepared and tested catalytically in the isobutene–methacrolein conversion. The objective was to determine whether α-$Bi_2Sn_2O_7$ was: (i) an acceptor, namely a phase whose catalytic properties depend on the action of spill-over oxygen, (ii) a donor, namely a phase displaying no intrinsic catalytic activity but controlling that of the former one, and (iii) a third possibility being that this pyrostannate might exhibit an intermediary behaviour, like SnO_2 [10].

We show in this paper that when $Bi_2Sn_2O_7$ is mixed with acceptor phases, cooperation between the two oxides occurs and several hypotheses are put forward and discussed to explain the synergetic effects. Because these cooperation effects could be assigned to a mutual contamination, to a surface enrichment of the catalyst in one oxide or to the eventual formation of new mixed phases by solid state reactions between the two starting oxides, all the catalysts were submitted to several characterization techniques before and after catalytic use in order to evidence any bulk or surface modifications. X-ray photoelectron spectroscopy was used to collect informations on the dispersion of the various phases present on the catalyst surface. More particularly, the atomic intensity ratios were determined for the various elements to get an idea of the surface stoichiometry of these catalysts and to evidence a possible contamination of coverage effect. The nature of the phases present in the samples after calcination or catalytic test was determined by X-ray diffraction and compared with the initial bulk composition of fresh catalysts, in order to control the eventual formation of a new compound. The catalysts were also characterized by scanning electron microscopy coupled with energy-dispersive X-ray analysis (SEM-EDX) to determine shape, size and composition of the particles, and to detect possible changes in their morphology during the test. Because the two mixed phases $Bi_2Mo_3O_{12}$ and Bi_2WO_6 are known as catalysts for the oxidation and ammoxidation of unsaturated hydrocarbons [13–17], they were also prepared and tested catalytically in the isobutene–methacrolein conversion.

2. Experimental

2.1. Preparation of the pure oxides

Bismuth pyrostannate, $Bi_2Sn_2O_7$, was obtained from a dispersion in *n*-heptane of pure tin(IV) oxide and bismuth(III) oxide in stoichiometric amounts. In this procedure, commercial Bi_2O_3 (JANSSEN, 99.9%) was first dispersed at room temperature, in 100 ml heptane (ACROS, 99+%) under ultrasonic stirring for 15 min. SnO_2, prepared by acidification of $SnCl_4{\cdot}5H_2O$ (JANSSEN, 98+%) [9], was then added to the former slurry and the mixture was submitted to further sonication for the same period. The solvent was then removed slowly under reduced pressure. The resulting powder was finally calcined at 1033 K for 20 h under controlled air flow (1 l min^{-1}). The specific surface areas of the ternary phase, as determined by BET, were in the range 1–3 $m^2\,g^{-1}$. The literature mentions that, under controlled conditions, three different bismuth pyrostannate phases exist depending on the temperature: α-$Bi_2Sn_2O_7$, probably tetragonal, stable below 363 K, β-$Bi_2Sn_2O_7$, cubic, appearing in the temperature range 363–953 K and γ-$Bi_2Sn_2O_7$, cubic, existing above 953 K [18]. However, X-ray

diffraction measurements carried out between 293 and 1033 K on our samples confirmed the presence of the α-phase in all the fresh and used catalysts throughout the investigated temperature range.

Molybdenum(VI) oxide was obtained by a complexation procedure from ammonium heptamolybdate (MERCK, 99%) and citric acid (MERCK, 99.5%) [19] and presented a specific surface area equal to 1.6 $m^2 g^{-1}$.

Antimony oxide, α-Sb_2O_4 (S_{BET}=0.7 $m^2 g^{-1}$) was prepared by calcination of Sb_2O_3 (MERCK, p.a.) under air at 773 K for 20 h [20]. Commercial bismuth and tungsten oxides (Bi_2O_3 JANSSEN, 99.9%; WO_3 JANSSEN, 99+%) were used for the mechanical mixtures with $Bi_2Sn_2O_7$. Their specific surface areas were 0.3 and 3 $m^2 g^{-1}$, respectively.

α-Bismuth molybdate, $Bi_2Mo_3O_{12}$, was prepared from an acidic solution containing ammonium heptamolybdate and pentahydrated bismuth nitrate (FLUKA, >99%) in the presence of citric acid (0.33 mol l^{-1}) [21]. After drying (373 K), the powder was calcined in air (1 l min^{-1}), first at 573 K for 20 h, then at 773 K for the same period and presented a final specific surface area of 1.7 $m^2 g^{-1}$.

To synthesize bismuth tungstate, Bi_2WO_6, commercial Bi_2O_3 and WO_3 were intimately mixed in a mortar and then calcined at 1173 K for three days. The presence of Bi_2WO_6 was checked by XRD and its BET specific surface area was shown to be 1.9 $m^2 g^{-1}$.

2.2. Preparation of the mechanical mixtures based on $Bi_2Sn_2O_7$

The biphasic catalysts $Bi_2Sn_2O_7$–MoO_3 and $Bi_2Sn_2O_7$–WO_3 were prepared by mechanical mixture of the two starting oxides in *n*-heptane under ultrasonic stirring according to the procedure described above. The engaged amounts were calculated to obtain a series of mixtures characterized by the following compositions: R_m =0.25, 0.50, 0.67, 0.75 and 0.91, where R_m refers to the weight ratio of bismuth pyrostannate in the mixture, i.e.

$$R_m = \text{wt } Bi_2Sn_2O_7/(\text{wt } Bi_2Sn_2O_7 + \text{wt B}),$$

where B = other oxide.

$Bi_2Sn_2O_7$–Sb_2O_4 and $Bi_2Sn_2O_7$–Bi_2O_3 mixtures corresponding to R_m=0.5 were prepared under the same conditions.

2.3. Calcination experiments

Further calcination experiments were carried out on the $Bi_2Sn_2O_7$–WO_3 and $Bi_2Sn_2O_7$–MoO_3 systems in order to examine whether ternary bismuth tungstate or molybdate phases could be generated under experimental conditions comparable to those of the catalytic test, and to look at the possible propensity of one phase to cover the other one. Mixtures corresponding to different compositions (R_m=0.25–0.91) were therefore calcined in the temperature range 673–1073 K and characterized by XRD, SEM-EDX and XPS.

2.4. Measurement of the catalytic activity

2.4.1. Catalytic tests

The catalytic performances of these catalysts were evaluated in the partial oxidation of isobutene into methacrolein, using air, in the temperature range 623–673 K. The experimental set-up includes a U-shaped fixed bed glass reactor (internal diameter 8 mm), temperature and mass flow regulation systems, and an on-line gas chromatograph for the analysis of the reagents and products. To maintain the isobutene conversion at moderate values, while keeping the total catalyst amount constant, the quantity of active phase was reduced to 62.5 wt% in all the catalysts, mechanical mixtures and pure oxides, by diluting the active phase with an extensively sintered silica calcined at 1273 K for 24 h (S_{BET} =0.5 $m^2 g^{-1}$), that was demonstrated to be inactive for the investigated reaction. The mass of catalyst (active phase+SiO_2) used for each run was fixed at 400 mg. Before their use in the catalytic tests, the catalysts (active phase+SiO_2) were pelletized into granules of 0.5–0.8 mm diameter. Reactants were introduced as a 3.4%, 20.3%, 76.3% volume mixture of isobutene, oxygen and nitrogen, respectively. Total gas flow was equal to 30 ml min^{-1}. Temperature control was ensured by chromel–alumel thermocouples. The composition of the gaseous mixture at the reactor output was analysed with a gas chromatograph INTERSMAT IGC 12M, equipped with two 2.5 m columns, the first one for the separation of isobutene, CO_2 and water (stationary phase PORAPAK), the other one for the analysis of partial oxidation products (stationary phase TENAX). Helium was used as carrier gas and detection was

made by catharometry. CO_2 and formaldehyde were found to be the major side products in all the catalytic tests and, together with methacrolein, accounted for the mass balance in the reactor. Traces of CO (<1%) were detected independently and carbonaceous deposits were evidenced at the surface of the used catalysts by XPS.

2.4.2. Expression of catalytic results

Catalytic results are expressed as isobutene conversion (X, %), yield in methacrolein (Y_{met}, %), selectivity in methacrolein (S_{met}, %) and yield in CO_2 (Y_{CO_2}, %). The conversion is defined as the ratio between the number of moles of isobutene converted and the number of moles of isobutene introduced. The yield in methacrolein represents the ratio of the number of moles of methacrolein formed to the initial number of moles of isobutene in the reactor. The yield in CO_2 will be tabulated as $Y_{CO_2}/4$ to take into account the formation of four moles of CO_2 per mole of isobutene converted. The selectivity in methacrolein is defined as the ratio between methacrolein yield and isobutene conversion ($S_{met}=Y_{met}/X$).

2.4.3. Quantitative evaluation of the synergetic effects

The differences between the specific surface areas of bismuth pyrostannate and those of the various oxides involved in the mixtures were not very important; nevertheless, to check whether the increase of catalytic performances in the mechanical mixtures might be assigned to a real cooperation effect, or merely reflects the change of the global specific surface area, we calculated the intrinsic yield, i.e. the yield normalized for a standard specific surface area of 1 $m^2\,g^{-1}$. The synergy on this parameter was then evaluated from the difference between the real intrinsic yield of the AB mixture, Y^*_{AB}, and the theoretical yield, $(Y^*_{AB})_{th}$ i.e. the yield that would be obtained in the absence of any cooperation, assuming zero-order reactions as a first approximation. Because it is impossible to measure the respective surface areas developed by each phase in the mixture, the calculation of the theoretical intrinsic yield $(Y^*_{AB})_{th}$ was based on a total surface area which is evaluated from the weighted sum of the respective surface areas of the two components. The considered parameters were defined in the following way:

1. Theoretical intrinsic yield of AB mixture, $(Y^*_{AB})_{th}$:

$$(Y^*_{AB})_{th} = [Y_A \cdot R_m + Y_B \cdot (1 - R_m)]/[(S_{BET})_A \cdot R_m + (S_{BET})_B \cdot (1 - R_m)], \quad (1)$$

where A=bismuth stannate, B=other oxide and $(S_{BET})_i$ is the specific surface area of the oxide i.

2. Real intrinsic yield of AB mixture, Y^*_{AB}:

$$Y^*_{AB} = [Y_{AB}]/[(S_{BET})_{AB}], \quad (2)$$

where $(S_{BET})_{AB}$ is the experimental specific surface area of the AB mixture and Y_{AB} is the experimental yield of the AB mixture.

3. Synergy on yield for the AB mixture, ΔY^*_{AB} (in %):

$$\Delta Y^*_{AB} = 100 \cdot [Y^*_{AB} - (Y^*_{AB})_{th}]/[(Y^*_{AB})_{th}]. \quad (3)$$

In the same way, we defined the intrinsic conversion, X^*_{AB}, which was normalized for a standard specific surface area of 1 $m^2\,g^{-1}$.The synergy on methacrolein selectivity is defined by the following expressions:

4. Theoretical selectivity, $(S_{AB})_{th}$:

$$(S_{AB})_{th} = [Y_A \cdot R_m + Y_B \cdot (1 - R_m)]/[X_A \cdot R_m + X_B \cdot (1 - R_m)]. \quad (4)$$

5. Real selectivity, S_{AB}:

$$S_{AB} = [Y_{AB}]/[X_{AB}], \quad (5)$$

where X_{AB} is the experimental conversion of the AB mixture.

6. Synergy on methacrolein selectivity, ΔS_{AB} (in %):

$$\Delta S_{AB} = 100 \cdot [S_{AB} - (S_{AB})_{th}]/[(S_{AB})_{th}]. \quad (6)$$

2.5. Physical characterization techniques

Powder X-ray diffraction (XRD) patterns were obtained with a SIEMENS D-5000 diffractometer using the Cu-K_α radiation (λ=154.18 pm). Phases were identified with reference to the JCPDS file.

X-ray photoelectron spectra were registered on a SSI-X-probe (SSX-100/206) spectrometer from FISONS, using a monochromatized Al-K_α radiation (E=1486.6 eV) and a ceramic sample holder. Charge compensation was achieved by the use of a flood gun fixed at 10 eV. The binding energy scale was calibrated with respect to the C1s photopeak of hydrocarbon contamination, taken at 284.8 eV. The analyses

of tin, bismuth, molybdenum, tungsten and oxygen were based on the following photopeaks: $Sn3d_{5/2}$, $Bi4f_{7/2}$, $Mo3d_{5/2}$, $W4f_{7/2}$ and O1s.

BET specific surface areas were measured with a MICROMERITICS ASAP 2000 apparatus at 77 K, using krypton as adsorbing gas.

Scanning electron microscopy was carried out on a LEICA Stereoscope S260 equipped for energy dispersive X-ray analysis (EDAX 9100). Samples were first dispersed in acetone and deposited on a Cu–Al sample-holder. Because of their non-conductive character, they were coated by a thin gold film in order to reduce charge effects.

3. Results and discussion

3.1. Catalytic results

The catalytic performances of the various samples towards the selective oxidation of isobutene into methacrolein are listed in Table 1. It suggests the following comments:

1. Pure bismuth stannate was found to display a poor catalytic activity for the considered reaction in the temperature range 648–673 K. Isobutene was slightly converted into formaldehyde and CO_2, but no methacrolein was produced.
2. No synergetic effects were evidenced in the $Bi_2Sn_2O_7$–Sb_2O_4 and $Bi_2Sn_2O_7$–Bi_2O_3 systems which were found to be completely inactive for the investigated reaction.
3. On the other hand, significant cooperative effects resulting in increased conversion, yield and selectivity in methacrolein were clearly observed in the mixture between bismuth stannate and molybdenum oxide.
4. Pure bismuth molybdate, α-$Bi_2Mo_3O_{12}$, was found to be active and selective for the considered reaction.
5. The systems containing bismuth stannate and tungsten oxide also resulted in positive cooperation effects on both the yield and the selectivity in methacrolein. The most selective catalyst was the mixture containing 75 wt% of $Bi_2Sn_2O_7$ (R_m=0.75). However, the WO_3-poor catalyst containing only 9.1 wt% WO_3 (R_m=0.91) was found to be essentially inactive and to produce no methacrolein. These $Bi_2Sn_2O_7$–WO_3 systems exhibit a lower intrinsic activity than those containing MoO_3. This can be explained by the difference in the catalytic potentialities of MoO_3 and WO_3, the latter oxide being well known to be a less performant catalyst for the partial oxidation of alkenes into oxygenated products [19]. Similarly, pure Bi_2WO_6 only showed a moderate activity and selectivity while $Bi_2Mo_3O_{12}$ is highly active and selective.

Figs. 1 and 2 describe the synergetic effects observed on methacrolein yield and selectivity in the $Bi_2Sn_2O_7$–MoO_3 catalysts.They show that synergy

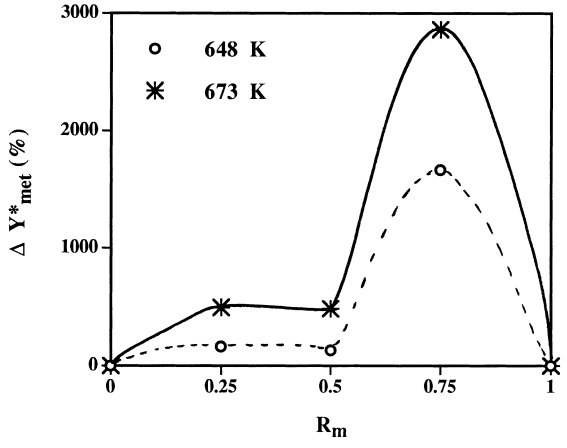

Fig. 1. Synergy on methacrolein yield in $Bi_2Sn_2O_7$–MoO_3 mixtures vs catalyst composition.

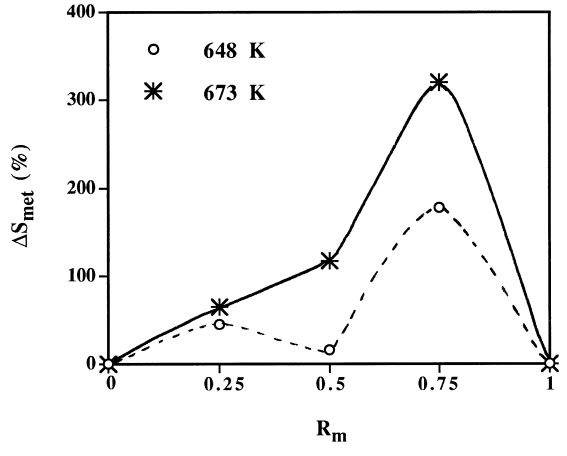

Fig. 2. Synergy on methacrolein selectivity in $Bi_2Sn_2O_7$–MoO_3 mixtures vs catalyst composition.

Table 1
Catalytic results normalized for a standard specific area of 1 $m^2\ g^{-1}$

Catalyst[a] $Bi_2Sn_2O_7$/B/R_m[b]	S_{BET}[c] ($m^2\ g^{-1}$)	T=648 K[d]				T=673 K[d]			
		X/S_{BET} (% g m^{-2})	Y_{met}/S_{BET} (% g m^{-2})	S_{met} (%)	$(Y/4)_{CO_2}/S_{BET}$ (% g m^{-2})	X/S_{BET} (% g m^{-2})	Y_{met}/S_{BET} (% g m^{-2})	S_{met} (%)	$(Y/4)_{CO_2}/S_{BET}$ (% g m^{-2})
SiO_2/-	0.5	—	—	—	—	2.4	0	0	0
$Bi_2Sn_2O_7$/-	3.1	1.0	0	0	0	4.8	0	0	1.3
MoO_3/-	1.6	9.7	3.1	32	0	10.5	3.9	38	0
$Bi_2Sn_2O_7/Sb_2O_4$/0.5	1.8	1.1	0	0	0[e]	1.4	0	0	0
$Bi_2Sn_2O_7/Bi_2O_3$/0.5	1.7	1.1	0	0	0[e]	1.5	0	0	0
$Bi_2Sn_2O_7/MoO_3$/0.25	1.8	10.9	4.9	45	0.72	27.9	15.2	54	3.4
$Bi_2Sn_2O_7/MoO_3$/0.5	2.4	7.4	2.5	34	1.2	14.5	8.3	57	5.1
$Bi_2Sn_2O_7/MoO_3$/0.75	2.7	12.6	8.7	69	2.1	26.3	18.2	69	6.9
$Bi_2Mo_3O_{12}$/-	1.7	8.4	4.8	57	0	28.4	16.5	58	3.6
$Bi_2Sn_2O_7$/-	1.0	3.0	0	0	0	4.8	0	0	0
WO_3/-	3.0	5.7	1.3	23	0.53	9.0	1.6	18	2.1
$Bi_2Sn_2O_7/WO_3$/0.25	2.4	5.9	1.7	28	0.25	9.6	2.1	23	1.8
$Bi_2Sn_2O_7/WO_3$/0.5	2.1	4.8	1.6	34	0	9.2	2.2	25	1.5
$Bi_2Sn_2O_7/WO_3$/0.67	1.8	3.2	1.4	37	0	6.1	1.7	23	1.4
$Bi_2Sn_2O_7/WO_3$/0.75	1.1	5.8	3.4	58	0	11.0	4.5	40	0.82
$Bi_2Sn_2O_7/WO_3$/0.91	1.0	4.6	0	0	0	7.5	0	0	0
Bi_2WO_6/-	1.9	3.3	1.3	38	0	6.6	2.5	38	0

[a]400 mg (250 mg of active phase+150 mg SiO_2) for all catalysts; 250 mg for pure SiO_2.
[b]R_m=wt $Bi_2Sn_2O_7$/(wt $Bi_2Sn_2O_7$+wt B) with B=other oxide.
[c]Experimental specific surface area of the active phase (without silica). These values were used to calculate the normalized catalytic results.
[d]Apart from CO_2, formaldehyde was found to be another by-product and accounted for the mass balance in the reactor. The formation of carbonaceous deposits was revealed by XPS analyses and, together with traces of CO (<1%), could consequently also complete, to a lower extent, the mass balance.
[e]At 623 K.

is especially important in the $Bi_2Sn_2O_7$-rich region and is still more pronounced at 673 K. Positive synergetic effects are also observed on both total isobutene conversion and CO_2 yield.

In the $Bi_2Sn_2O_7$–WO_3 catalysts, the synergy on methacrolein yield and selectivity is similarly the highest in the $Bi_2Sn_2O_7$-rich mixture but is unaffected by the reaction temperature (Figs. 3 and 4). The synergetic effects on aldehyde yield are however less pronounced than in the $Bi_2Sn_2O_7$–MoO_3 system. Synergy on isobutene conversion and CO_2 yield (Figs. 5 and 6) are rather low or even negative.

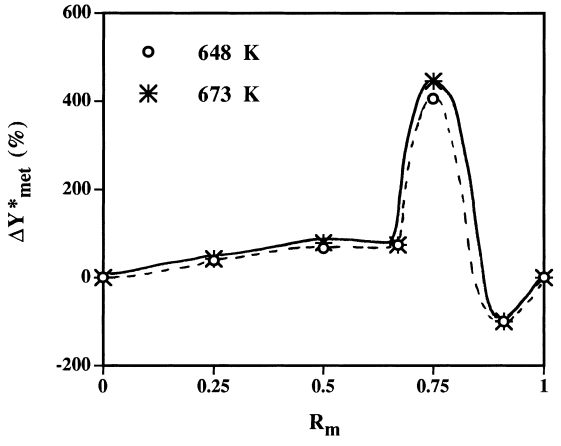

Fig. 3. Synergy on methacrolein yield in $Bi_2Sn_2O_7$–WO_3 mixtures vs catalyst composition.

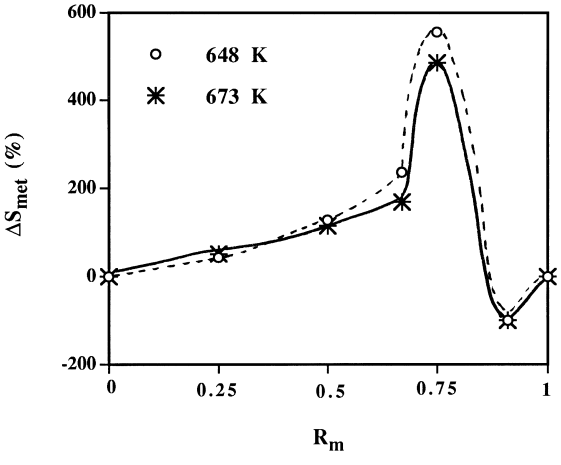

Fig. 4. Synergy on methacrolein selectivity in $Bi_2Sn_2O_7$–WO_3 mixtures vs catalyst composition.

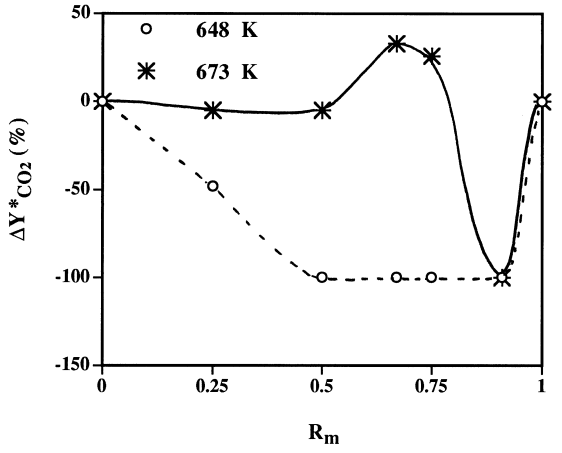

Fig. 5. Synergy on CO_2 yield in $Bi_2Sn_2O_7$–WO_3 mixtures vs catalyst composition.

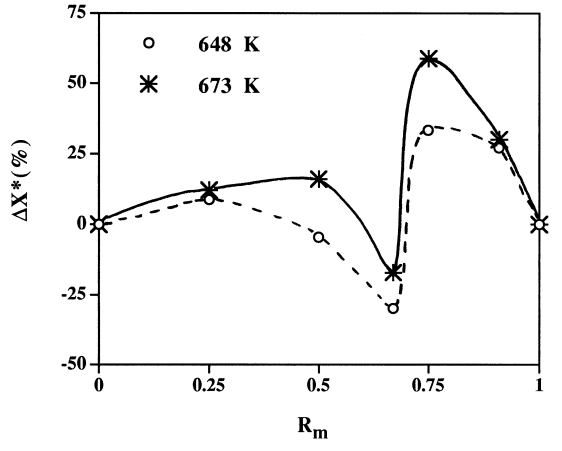

Fig. 6. Synergy on isobutene conversion in $Bi_2Sn_2O_7$–WO_3 mixtures vs catalyst composition.

3.2. Physico-chemical characterization of the catalysts

3.2.1. XRD

Whereas in the $Bi_2Sn_2O_7$–MoO_3 mixtures, the ternary α-bismuth molybdate, α-$Bi_2Mo_3O_{12}$, was detected in low quantities in the used catalysts, the presence of any mixed phase (tungstate) was never revealed after the catalytic test in the $Bi_2Sn_2O_7$–WO_3 samples.

Table 2 shows the influence of the calcination temperature on the nature of the different crystalline phases identified by X-ray diffraction.

Table 2
XRD characterization of the catalysts

Catalyst $Bi_2Sn_2O_7$/B/R_m[a]	Calcination temperature (K)[b]	Phases detected by XRD[c]			
$Bi_2Sn_2O_7/MoO_3$/0.5	673	$Bi_2Sn_2O_7$	MoO_3	$Bi_2Mo_3O_{12}$*ff*	SnO_2*ff*
$Bi_2Sn_2O_7/MoO_3$/0.5	773	$Bi_2Sn_2O_7$	MoO_3	$Bi_2Mo_3O_{12}$*f*	SnO_2*ff*
$Bi_2Sn_2O_7/MoO_3$/0.5	873	MoO_3	$Bi_2Mo_3O_{12}$	SnO_2*m*	
$Bi_2Sn_2O_7/MoO_3$/0.5	973	MoO_3	$Bi_2Mo_3O_{12}$	SnO_2*m*	
$Bi_2Sn_2O_7/MoO_3$/0.5	1033	MoO_3	$Bi_2Mo_3O_{12}$	SnO_2*m*	
$Bi_2Sn_2O_7/WO_3$/0.25	873	$Bi_2Sn_2O_7$	WO_3		
$Bi_2Sn_2O_7/WO_3$/0.25	973	$Bi_2Sn_2O_7$	WO_3	Bi_2WO_6*ff*	
$Bi_2Sn_2O_7/WO_3$/0.5	673	$Bi_2Sn_2O_7$	WO_3*m*		
$Bi_2Sn_2O_7/WO_3$/0.5	873	$Bi_2Sn_2O_7$	WO_3*f*		
$Bi_2Sn_2O_7/WO_3$/0.5	973	$Bi_2Sn_2O_7$	WO_3*f*	Bi_2WO_6*f*	SnO_2*f*
$Bi_2Sn_2O_7/WO_3$/0.5	1073	Bi_2WO_6	WO_3*f*	$Bi_2Sn_2O_7$*m*	SnO_2*m*
$Bi_2Sn_2O_7/WO_3$/0.67	873	$Bi_2Sn_2O_7$	WO_3*f*		
$Bi_2Sn_2O_7/WO_3$/0.67	973	$Bi_2Sn_2O_7$	WO_3*f*	Bi_2WO_6*f*	
$Bi_2Sn_2O_7/WO_3$/0.75	873	$Bi_2Sn_2O_7$	WO_3*f*	Bi_2WO_6*ff*	
$Bi_2Sn_2O_7/WO_3$/0.75	973	$Bi_2Sn_2O_7$	WO_3*f*	Bi_2WO_6*f*	
$Bi_2Sn_2O_7/WO_3$/0.91	873	$Bi_2Sn_2O_7$	WO_3*ff*		
$Bi_2Sn_2O_7/WO_3$/0.91	973	$Bi_2Sn_2O_7$	SnO_2*ff*	Bi_2WO_6*f*	

[a] R_m=wt $Bi_2Sn_2O_7$/(wt $Bi_2Sn_2O_7$+wt B) with B=other oxide.
[b] During 20 h.
[c] Phases detected in a low amount are noted, by decreasing order: *m*>*f*>*ff*.

The XRD analyses revealed traces of bismuth molybdate, α-$Bi_2Mo_3O_{12}$, after calcination at 673 K. Quantitative conversion into this phase was observed above 873 K.

On the other hand, the formation of γ-bismuth tungstate, Bi_2WO_6, only appears above 873 K in a very low amount and its presence is clearly established at 973 K only. In a 1/1 $Bi_2Sn_2O_7$–WO_3 mixture, γ-bismuth tungstate was found to become the major phase above 1073 K. Any other Bi–W–O phase was never detected in our calcined samples. These experiments confirm thus the fact that, contrary to the case of the bismuth molybdates for which the formation temperatures are rather low, the bismuth tungstates do not form very easily and only appear after calcination above 873 K. The requirements for high temperatures to synthesize mixed Bi–W–O phases are mentioned in the literature [22–24], and were a key point to suggest the use of WO_3 as oxygen spill-over acceptor in the present work. To establish the donor character of $Bi_2Sn_2O_7$, it was indeed essential to choose acceptors in a relevant way, in order to obtain a system which would not easily induce the formation of new mixed phases that might be catalytically active.

3.2.2. BET specific surface area

As indicated in Table 1, the experimental specific surface areas of the various mixtures are in agreement with the values which could be calculated from the respective specific surface areas of the constituting oxides. This observation suggests that the procedure followed to prepare the mechanical mixtures does not induce any significant change of the size and morphology of the starting particles. When the $Bi_2Sn_2O_7$–MoO_3 mixtures are calcined up to 1033 K, there is a 40% decrease in the specific surface area which is thought to reflect mainly a classical sintering effect, without any clear evidence of spreading or morphological change.

3.2.3. SEM-EDX

Because the explanation of the SEM-EDX results is easier in the case of the $Bi_2Sn_2O_7$–WO_3 systems than in the corresponding ones containing MoO_3, we will begin with the presentation of the former.

3.2.3.1. $Bi_2Sn_2O_7$–WO_3 systems. While tungsten oxide particles appear as large smooth crystallites (30–160 μm), the $Bi_2Sn_2O_7$ particles are small (a few μm) and spongy. When these two oxides are

mixed, their morphology remains the same and the WO_3 crystallites are decorated by bismuth stannate particles. The dispersion of these ones seems however to decrease in the calcined samples when the temperature increases above 673 K, in such a way that tungsten oxide appears either naked or inhomogeneously ornamented. In the mixture containing 75% $Bi_2Sn_2O_7$ (R_m =0.75), this inhomogeneity is already observed in the uncalcined catalyst. The presence of particles containing simultaneously Bi and W is clearly evidenced by EDX in the samples where Bi_2WO_6 was revealed by XRD to become the major product (mixture calcined at 1073 K).

After the catalytic test, the morphology and the composition of the catalysts are unchanged when comparing with the corresponding sample before test.

3.2.3.2. $Bi_2Sn_2O_7$–MoO_3 systems. The interpretation of the SEM images of MoO_3-containing samples is rather difficult because of the wide diversity in the morphology of MoO_3 particles. Indeed, pure molybdenum oxide appears curiously, either like very small particles (<10 μm), free or agglomerated, or like very long lamellas (140–290 μm). The latter are sometimes smooth but often decorated by small planes (a few μm) and can present step-like fractures.

The SEM pictures of the $Bi_2Sn_2O_7$–MoO_3 mixtures display a great number of small MoO_3 particles with from time to time, a free lamella or a mass containing simultaneously both intermixed lamellas, spongy agglomerates made of small molybdenum oxide and stannate particles, and, occasionnally, crystallites (25–90 μm). The latter seem to consist either in molybdenum oxide decorated by stannate particles or more often in pure bismuth stannate. Calcination at 673 K does not alter the morphology of the oxide particles. However, the SEM-EDX technique was found to give indication in detecting the generation of a ternary Bi–Mo–O phase from 873 K, first as small particles (a few μm), then as large rough ones (20–210 μm) when the temperature was increased up to 1023 K.

SEM pictures of samples after test show that their general morphology remains relatively the same as initially. We have, however, to note the reduced size of the molybdenum oxide lamellas (20–50 μm).

3.2.4. XPS

The binding energy values (E_b) of the analytical peaks in pure $Bi_2Sn_2O_7$, MoO_3 and WO_3 are 486.2, 159.1, 233.2, 35.4 and (530.0±0.3) eV for tin, bismuth, molybdenum, tungsten and oxygen, respectively. In mechanical mixtures, the E_b values of these elements slightly differ from the previous values and appear in the range (486.2–487.0), (159.2–159.8), (232.5–233.2), (35.4–35.9) and (529.9–530.9) eV, respectively. These values remain the same after calcination or use in the catalytic tests, and there is no indication of the presence of new oxidation states.

The XPS data obtained for the $Bi_2Sn_2O_7$–MoO_3 and $Bi_2Sn_2O_7$–WO_3 systems are listed in Tables 3 and 4, respectively. We have to note that the analysis of these results is particularly difficult and could consequently be incomplete. Nevertheless, we will try to give an interpretation as accurate as possible. First, we would like to remember that the intensity ratios can depend on several factors, namely:

1. The difference in the particle size of each oxide, which can in turn be modified during the catalytic test. Initial small particles which give rise to an enhanced XPS signal can, indeed, undergo sintering during the catalytic use, resulting in decreased intensities.
2. The surface contamination of one phase by metallic elements from the other phase.
3. The formation of a monolayer (or multilayer) of one phase on the surface of the other.
4. The formation of a new compound during the test.
5. The deposition during the catalytic test of a thick carbon film on the oxide surface, which can be predominant on one of the partners and consequently affect the intensity of the photoelectrons with low kinetic energy (high binding energy).

3.2.4.1. $Bi_2Sn_2O_7$–MoO_3 systems. Table 3 reports the XPS atomic ratios of $Bi_2Sn_2O_7$–MoO_3 samples and suggests the following comments:

1. First, any coverage effect of MoO_3 on $Bi_2Sn_2O_7$ in fresh, i.e. uncalcined and untested, samples might apparently be ruled out because the experimental atomic intensity ratios Sn/Mo and Bi/Mo correspond to the theoretical bulk values. In the same way, the XPS data collected after various calcination treatments did not indicate any coverage of bismuth stannate by molybdenum oxide. It is

Table 3
Atomic intensity ratios measured by XPS in $Bi_2Sn_2O_7$–MoO_3 mixtures

R_m[a]	Bulk values Bi/Mo=Sn/Mo	Calcination temperature (K)	Fresh catalysts						Used catalysts					
			Bi/Sn	Sn/Mo	Bi/Mo	C/Sn	C/Bi	C/Mo	Bi/Sn	Sn/Mo	Bi/Mo	C/Sn	C/Bi	C/Mo
0.25[b]	0.13	—	0.96	0.16	0.15	8.8	9.2	1.4	0.64	0.17	0.11	16.8	26.3	2.9
0.5[b]	0.37	—	0.75	0.20	0.15	6.3	8.4	1.3	0.68	0.20	0.13	16.4	24.3	3.2
0.75[b]	1.1	—	0.88	1.1	0.97	2.0	2.3	2.2	0.64	0.77	0.50	5.6	8.8	4.4
0.5	0.37	—	1.3	0.30	0.39	4.7	3.5	1.4						
		673	0.89	0.36	0.32	3.9	4.3	1.4						
		773	0.54	0.40	0.22	3.4	6.2	1.4						
		873	1.0	0.37	0.37	3.9	3.9	1.5						
		973	1.1	0.32	0.37	4.5	4.0	1.5						
		1033	0.91	0.48	0.44	3.3	3.6	1.6						

[a] R_m=wt $Bi_2Sn_2O_7$/(wt $Bi_2Sn_2O_7$+wt MoO_3).
[b] Systems which have been submitted to catalytic tests and were consequently mixed with silica.

Table 4
Atomic intensity ratios measured by XPS in $Bi_2Sn_2O_7$–WO_3 mixtures

R_m[a]	Bulk values Bi/W=Sn/W	Calcination temperature (K)	Fresh catalysts						Used catalysts					
			Bi/Sn	Sn/W	Bi/W	C/Sn	C/Bi	C/W	Bi/Sn	Sn/W	Bi/W	C/Sn	C/Bi	C/W
0[b,c]	—	—	—	—	—	—	—	1.8	—	—	—	—	—	7.2
0[b]	—	[d]	—	—	—	—	—	2.1						
0.25[c]	0.2	—	1.0	0.28	0.28	8.9	8.9	2.4	1.2	0.29	0.35	23.2	19.2	6.7
0.25	0.2	—	1.1	0.33	0.38	4.4	3.9	1.5						
		873	1.1	0.36	0.39	4.7	4.3	1.7						
		973	1.2	0.35	0.41	4.9	4.3	1.7						
0.5[c]	0.6	—	1.1	2.1	2.3	3.1	2.9	6.5	1.3	0.51	0.65	14.4	11.3	7.3
0.5	0.6	—	0.91	3.1	2.8	1.7	1.8	5.1						
		673	1.5	1.1	1.7	2.0	1.3	2.3						
0.5	0.6	—	0.96	1.6	1.5	2.0	2.1	3.1						
		873	1.2	0.93	1.1	2.2	1.8	2.0						
		973	1.2	0.85	1.0	2.3	1.9	1.9						
		1073	1.4	0.85	1.1	2.4	1.8	2.0						
0.67[c]	1.2	—	1.1	2.0	2.2	2.9	2.6	5.9	1.2	2.1	2.4	4.3	3.7	8.9
0.67	1.2	—	1.3	3.8	5.0	1.6	1.2	6.1						
		873	1.4	1.2	1.8	2.2	1.6	2.7						
		973	1.5	0.98	1.5	2.2	1.4	2.1						
0.75[c]	1.8	—	1.1	2.2	2.5	3.1	2.8	6.8	1.3	1.7	2.1	5.8	4.6	9.7
0.75	1.8	—	1.2	1.6	2.0	1.8	1.5	2.9						
		873	1.5	0.97	1.5	2.1	1.4	2.1						
		973	1.7	0.95	1.6	2.8	1.6	2.7						
0.91[c]	6.0	—	1.3	8.5	11.1	2.9	2.2	24.8	1.3	8.4	10.7	2.5	1.9	21.0
0.91	6.0	—	1.2	15.6	19.3	1.4	1.1	21.6						
		873	1.5	5.0	7.2	1.7	1.2	8.3						
		973	1.4	3.0	4.1	1.6	1.1	4.6						

[a] R_m=wt $Bi_2Sn_2O_7$/(wt $Bi_2Sn_2O_7$+wt WO_3).
[b] R_m=0 corresponds to pure WO_3.
[c] Systems which have been submitted to catalytic tests and were consequently mixed with silica.
[d] Deposition in *n*-heptane.

clearly shown in the 1/1 $Bi_2Sn_2O_7$–MoO_3 mixture (R_m=0.5) for which the atomic intensity ratios Sn/Mo and Bi/Mo do not change significantly with the calcination temperature and remain consistent with the theoretical values. The $Bi_2Sn_2O_7$–MoO_3 system can consequently be qualified as showing no propensity to mutual contamination or monolayer formation, even after thermal treatment.

2. On the other hand, in the catalysts after test, the modifications of the Sn/Mo and Bi/Mo intensity ratios could probably be explained by the presence of an important carbon deposit on the oxides, preferentially on $Bi_2Sn_2O_7$. But similarly, no propensity to coverage or contamination seems to appear.

3.2.4.2. $Bi_2Sn_2O_7$–WO_3 systems. XPS atomic intensity ratios of $Bi_2Sn_2O_7$–WO_3 catalysts are listed in Table 4; the influence of several factors which could modify these atomic ratios is discussed in order to elucidate some peculiarities in the experimental data and to evidence a possible contamination effect.

(i) *Influence of the preparation method on the carbon contamination*: In order to determine whether the preparation method of the catalysts by mechanical mixture in an hydrocarbon does not lead to carbon contamination, we submitted pure tungsten oxide to a dispersion procedure in *n*-heptane without adding any bismuth stannate. This sample was found to contain only minor amounts of carbon (line 2), indicating that this step of the preparation procedure cannot be taken as responsible for the presence of these surface carbonaceous species.

(ii) *Influence of the catalytic tests on the metal atomic intensity ratios*: For all the catalysts, we can claim that the catalytic test does not induce measurable modifications of the atomic intensity ratios presented by the starting materials: the Sn/W and Bi/W intensity ratios observed after test are similar to those observed in the corresponding fresh catalysts. This is valid for all the samples but one (R_m =0.5), for which the modifications of the XPS ratios can be explained by the preferential coke deposition on bismuth stannate during the catalytic test.

(iii) *WO_3-rich catalysts*: In all the WO_3-rich catalysts (R_m =0.25–0.67), calcined, used and even fresh, the Bi/W and Sn/W values are found to be systematically larger than the theoretical ones. This could "a priori" be explained either by a significant difference in the particle size of the two oxides or by a coverage phenomenon of WO_3 by $Bi_2Sn_2O_7$. The first hypothesis seems to be the most pertinent one, because SEM measurements revealed that bismuth stannate particles are small (a few μm) while tungsten oxide appears like very large crystallites (30–60 μm); the XPS signals of the latter are therefore weakened with respect to those of $Bi_2Sn_2O_7$. On the other hand, if a contamination is responsible for these peculiarities, the effect would be increased after calcination of the mixtures, and this is not the case: the calcination experiments do not produce any significant modification of the atomic intensity ratios between the metals, indicating that surface enrichment does not seem to occur in these WO_3-rich samples. In any case, we can affirm that the catalytic test does not involve any modification of the starting catalyst.

(iv) *$Bi_2Sn_2O_7$−rich catalysts*: The results obtained for the $Bi_2Sn_2O_7$-rich mixtures ($R_m \geq 0.75$) are completely different. In the fresh (non-calcined) and tested catalysts, the Sn/W and Bi/W ratios are again larger than the bulk values, and this could be again explained by differences in the crystallite size of the oxides. However, in the calcined catalysts, these atomic intensity ratios (especially Sn/W) become definitely lower than the theoretical values. Two main hypotheses can be put forward to provide an explanation for this observation made on catalysts after calcination

- surface enrichment of the catalyst by WO_3,
- sintering of the stannate particles.

Possible contamination of $Bi_2Sn_2O_7$ by WO_3 cannot be immediately excluded but this tendency was neither observed in the calcined WO_3-rich mixtures ($R_m \leq 0.67$), nor in the used catalysts. This hypothesis must therefore be considered with great care.

The second hypothesis, namely sintering of the bismuth stannate particles, could be the most reasonable one if one refers to the SEM pictures of the $Bi_2Sn_2O_7$–WO_3 mixture with R_m =0.75. The SEM experiments performed on this $Bi_2Sn_2O_7$-rich system actually revealed a particularly poor dispersion of the stannate particles on tungsten oxide crystallites.

An additional third hypothesis could be the formation, during these calcination steps, of a preferential

coke deposit on bismuth stannate but it seems quite unreasonable: eventual carbonaceous species should normally be burned up upon calcination, as indicated by the experimental C/Sn and C/Bi ratios which are rather low. However, a residual carbon contamination could influence the metal intensity ratios, especially that of tin (electrons with higher E_b), explaining therefore the difference between the Sn/W and Bi/W ratios. In any case, this low carbon contamination only cannot account reasonably for the peculiarities observed in these samples.

As far as the $Bi_2Sn_2O_7$–WO_3 catalysts are concerned, the main conclusions related to the XPS results may be summarized as follows:

- In the WO_3-rich mixtures ($R_m \leq 0.67$), no contamination or coverage effect seems to occur between the two oxides; the discrepancy between the experimental Sn/W and Bi/W ratios and the theoretical bulk values observed in fresh, calcined or used catalysts is probably due to differences in the particle sizes of bismuth stannate and tungsten oxide.
- In the $Bi_2Sn_2O_7$-rich catalysts ($R_m \geq 0.75$), the situation is more confused and, in addition to the influence exerted by the morphological differences of the oxide particles, two hypotheses have to be retained to explain the XPS results of the calcined samples, namely, either a surface enrichment by WO_3, or a poor interdispersion of the two oxide particles.
- In any case, the catalytic tests do apparently not trigger significant modifications of the XPS intensity ratios. If some ''anomalies'' exist, they are already observed in the fresh catalysts, except in the mixture characterized by $R_m = 0.5$, for which a preferential carbon deposition on $Bi_2Sn_2O_7$ seems to occur during the catalytic use.

4. General comments and conclusions

$Bi_2Sn_2O_7$–Bi_2O_3 and $Bi_2Sn_2O_7$–Sb_2O_4 systems were found to be completely inactive for the selective oxidation of isobutene into methacrolein. On the other hand, positive cooperation effects for methacrolein production were observed when bismuth stannate was mixed with either tungsten or molybdenum oxide. Several phenomena might account for these synergetic effects, namely:

- in situ formation of a new mixed phase,
- surface enrichment by one of the oxides or mutual contamination,
- physical modifications of the catalysts particles (decrease of the particle sizes, deflocculation of aggregates),
- existence of a remote control mechanism.

Each of these possibilities was discussed to shed light on the mechanism of the cooperation existing in these biphasic catalysts.

4.1. $Bi_2Sn_2O_7$–WO_3

γ-bismuth tungstate, Bi_2WO_6, has been examined as catalyst for the oxidation and ammoxidation of alkenes in several studies, but it was revealed to be not as catalytically active as its molybdate counterpart in spite of the similarities in the structural chemistry of these phases [16]. The same conclusion can be drawn from the catalytic test performed in this work with pure Bi_2WO_6, which appeared to be moderately active and selective. However, XRD never revealed the presence of a new bismuth tungstate phase in the catalysts after test. Furthermore, additional calcination experiments confirmed the fact that Bi–W–O phases do not form easily (only above 873 K). It could be argued that the present results are limited by the sensitivity of the characterization technique and that small amounts of mixed tungstate would remain undetected by XRD. However, the literature confirms the difficulty to generate bismuth tungstates, and, in addition, the EDX results never revealed the appearance of a new compound during the catalytic test. This possibility seems thus to be very unlikely.

A second hypothesis involving physical changes in the morphology of the oxide particles may easily be discarded. Indeed, the SEM pictures did not reveal such changes either during the preparation of the mixture, or after the use in the catalytic tests.

The hypothesis of a contaminating layer must be discussed with greater care. In the WO_3-rich mixtures, the XPS results do not seem to evidence such phenomena, as well before as after test or calcination. In the $Bi_2Sn_2O_7$-rich samples, surface enrichment by WO_3 does apparently not take place during the catalytic test, but may however not be excluded after the

calcination steps. It appears thus rather unprobable that the aforementioned assumption reasonably accounts for the synergetic effects.

On the other hand, the results obtained for the $Bi_2Sn_2O_7$–WO_3 system could be easily explained within the framework of the remote control theory. Indeed, because WO_3 is known as a typical acceptor of spill-over oxygen, and because $Bi_2Sn_2O_7$ alone is inactive and does not cooperate with typical oxygen donors (Bi_2O_3, Sb_2O_4), this ternary oxide may be considered as a donor phase with respect to tungsten oxide.

4.2. $Bi_2Sn_2O_7$–MoO_3

The presence of bismuth molybdate in a low quantity has been revealed by the XRD analyses performed on used $Bi_2Sn_2O_7$–MoO_3 catalysts. Because this mixed phase is well known to be highly active and selective in partial oxidation and ammoxidation of propene, and also in oxidation of isobutene, as confirmed in the present work, it may therefore play a role in the synergy described above.

On the other hand, it appears that surface enrichment by one phase or mutual contamination of the two oxides might apparently be ruled out on the basis of the XPS results.

In spite of the in situ generation of $Bi_2Mo_3O_{12}$, the existence of a remote control mechanism between bismuth stannate and molybdenum oxide does not have to be merely excluded. $Bi_2Sn_2O_7$ seems indeed to behave as a donor phase with respect to WO_3; MoO_3 being similarly a typical acceptor phase, a synergy between this oxide and $Bi_2Sn_2O_7$ could occur independently from the formation of bismuth molybdate.

We will therefore conclude that two hypotheses can be retained to explain the synergetic effects observed in the $Bi_2Sn_2O_7$–MoO_3 system:

- the intrinsic catalytic activity of α-$Bi_2Mo_3O_{12}$,
- a remote control mechanism between $Bi_2Sn_2O_7$ (donor) and MoO_3 (acceptor).

Additional experiments on these mixtures are necessary to examine the possible role played by α-$Bi_2Mo_3O_{12}$ and to have a better knowledge of the mechanisms governing the cooperation effects in these complex multiphasic catalysts. Therefore, in a future investigation, we will focus on the catalytic behaviour of pure $Bi_2Mo_3O_{12}$ and of its mixture with $Bi_2Sn_2O_7$ or MoO_3, which will be the subject of a forthcoming paper.

References

[1] B. Delmon, P. Ruiz, S.R.G. Carrazán, S. Korili, M.A. Vicente Rodriguez, Z. Sobalik, in: M. Absi-Halabi, J. Beshara, H. Qabazard, A. Stanislaus (Eds.), Catalysts in Petroleum Refining and Petrochemical Industries 1995, Elsevier, Amsterdam, 1996, p. 1.
[2] P. Ruiz, B. Delmon, Catal. Today 3 (1988) 199.
[3] E.G. Gamid-Zade, E.A. Mamedov, R.G. Rizaev, Kinet. Katal. 20 (1979) 405.
[4] E.A. Mamedov, E.G. Gamid-Zade, F.M. Agaev, R.G. Rizaev, Kinet. Katal. 20 (1979) 410.
[5] E.A. Mamedov, G.W. Keulks, F.A. Ruzala, J. Catal. 70 (1981) 241.
[6] T. Seiyama, T. Uda, I. Mochida, E. Egashira, J. Catal. 34 (1974) 29.
[7] Y. Okamoto, K. Oh-Hiraki, T. Imanaka, S. Teranishi, J. Catal. 71 (1981) 99.
[8] C.A. Mims, A.J. Jacobson, R.B. Hall, J.T. Lewandowski, J. Catal. 153 (1995) 197.
[9] L. Moens, P. Ruiz, B. Delmon, M. Devillers, Catal. Lett. 46 (1997) 93.
[10] L.T. Weng, P. Ruiz, B. Delmon, Stud. Surf. Sci. Catal. 72 (1992) 399.
[11] L.T. Weng, P. Ruiz, B. Delmon, D. Duprez, J. Mol. Catal. 52 (1989) 349.
[12] L.T. Weng, E. Sham, B. Doumain, P. Ruiz, B. Delmon, Stud. Surf. Sci. Catal. 55 (1990) 757.
[13] M. El Jamal, M. Forissier, G. Coudurier, React. Kinet. Catal. Lett. 37 (1988) 349.
[14] D. Carson, M. Forissier, J.C. Vedrine, J. Chem. Soc., Faraday Trans. I 80 (1984) 1017.
[15] J.D. Burrington, R.K. Grasselli, J. Catal. 59 (1979) 79.
[16] L.Y. Margolis, E.K. Enikeev, O.V. Isaev, A.V. Krylova, M.Y. Kushnerov, Kinet. Katal. 3 (1962) 181.
[17] P. Sherwood, Ind. Chem. 39 (1963) 242.
[18] R.D. Shannon, J.D. Bierlein, J.L. Gilson, G.A. Jones, A.W. Sleight, J. Phys. Chem. Solids 41 (1980) 117.
[19] M. Devillers, O. Tirions, L. Cadus, P. Ruiz, B. Delmon, J. Solid State Chem. 126 (1996) 152.
[20] C. Li, Q. Xin, P. Ruiz, X.X. Guo, B. Delmon, J. Mol. Catal. 72 (1992) 307.
[21] F.Y. Qiu, L.T. Weng, P. Ruiz, B. Delmon, Appl. Catal. A 47 (1989) 115.
[22] S.N. Hoda, L.L.Y. Chang, J. Am. Ceram. Soc. 57 (1974) 323.
[23] E.L. Gal'Perin, L.Y. Erman, I.K. Kolchin, M.A. Belova, K.S. Chernyshev, Russ. J. Inorg. Chem. 11 (1966) 1137.
[24] D.A. Jefferson, J. Gopalakrishnan, A. Ramanan, Mat. Res. Bull. 17 (1982) 269.